Motagh, M., Klotz, J., Tavakoli, F., Djamour, Y, Arabi, S., Wetzel, H.-U., Zschau, J. (2006): Combination of precise leveling and InSAR data to constrain source parameters of the Mw = 6.5, 26 December 2003 Bam earthquake. - Pure and Applied Geophysics, 163, 1, 1-18,

DOI: 10.1007/s00024-005-0005-y.
URL: http://www.copernicus.org/EGU/annales/22/2/417.htm

Combination of Precise Leveling and InSAR Data to Constrain Source Parameters of the $M_w = 6.5$, 26 December 2003 Bam Earthquake

Mahdi Motagh,[1] Jürgen Klotz,[1] Farokh Tavakoli,[2] Yahya Djamour,[3] Siavash Arabi,[3] Hans-ulrich Wetzel,[1] and Jochen Zschau[1]

Abstract—We used new precise leveling data acquired 40 days after the Bam earthquake in combination with radar interferometry observations from both ascending and descending orbits to investigate static deformation associated with the 2003 Bam earthquake. We invert this geodetic data set to gain insight into the fault geometry and slip distribution of the rupture. The best-fitting dislocation model is a steeply east-dipping right-lateral strike-slip fault that has a size of 11 by 8 km and strikes N2°W. We find that such smooth geometry fits available geodetic data better than previously proposed models for this earthquake. Our distributed slip model indicates a maximum strike slip of 3 m occurring about 3 to 5 km deep. The slip magnitude and depth of faulting taper to the north, where the fault approaches the Bam city. Inclusion of crustal layering increases the amount of maximum slip inferred at depth by about 4%.

Key words: InSAR, leveling.

1. Introduction

The 25 December, 2003 ($M_w = 6.5$) Bam earthquake occurred in a region that experienced no great historical earthquake during the last 2000 years (Mostafazadeh *et al.*, 2004). Nevertheless, it is one of the most destructive events to strike southeastern Iran over the past 30 years. The city of Bam itself is located in the southern part of the Lut Block, where the apparent lack of seismicity suggests that it might be a relatively rigid block inside a distributed deformation zone in central Iran (Berberain *et al.*, 2001). The results of recent regional-scale GPS measurements, carried out between 1999 and 2001, also predict relatively low rates of right-lateral strike slip of about 9 mm/yr, 7 mm/yr and 3mm/yr along the eastern,

[1]GeoForschungsZentrum Potsdam (GFZ), Telegrafenberg, D-14473, Potsdam, Germany.
[2]Laboratoire de Geophysique Interne et Tectonophysique, Maison des Geosciences, BP 53, 38041, Grenoble Cedex 9, France.
[3]National Cartographic Center of Iran (NCC), Azadi Square, Meraj Avenue, P.O.Box: 13185–1684, Tehran, Iran.

southwestern and northwestern borders of the Lut block, respectively (VERNANT *et al.*, 2004).

Several studies have already been carried out to investigate mechanics and source parameters of the Bam earthquake. ZARE and HAMZEHLLOO (2004) analyzed strong motion records at 22 stations of the national Iranian strong motion network and concluded that a length of about 10 km of the previously-mapped Bam fault passing exactly from the east of the Bam city was ruptured during the earthquake. Preliminary aftershock locations from 29 December, 2003 to 30 January, 2004 showed a nearly vertical alignment of aftershocks located between 6 and 20 km depth on a 30 km north-south striking fault (TATAR *et al.*, 2004). FU *et al.* (2004) used Aster 3-D images and suggested that the Bam event was probably triggered by right-lateral strike-slip faulting on the northern segment of the Bam fault. TALEBIAN *et al.* (2004) examined Envisat ASAR data in descending orbit and argued that a combination of two mechanisms is necessary to fit InSAR observations; a vertical strike-slip dislocation approximately 5 km west of the Bam fault and a pure thrust dislocation beneath the Bam fault. WANG *et al.* (2004) inverted descending and ascending interferograms and concluded that the Bam event was a right-lateral strike-slip earthquake that ruptured a total length of about 24 km from south to north crossing the Bam city. WANG *et al.* (2004) found no evidence for secondary thrust dislocation as proposed by TALEBIAN *et al.* (2004).

In this paper we complement previous studies on the Bam earthquake using new precise leveling data acquired 40 days after the event in combination with InSAR measurements. The precise leveling data provide the most accurate observations of earthquake-induced surface deformation in the vertical component, allowing for precise calibration of the information obtained by the space-based InSAR technique. This combination enables us to constrain the geometry of dislocation caused by the Bam earthquake and resolve the discrepancy between the results obtained by previous studies for this event.

2. Data

2.1 Precise Leveling

The 2003 Bam earthquake occurred within a subset of precise-leveling stations that was first measured in 1988 as part of a program to establish the Iranian first-order leveling network across the country. In the 40 days following the earthquake, a leveling survey was undertaken by the National Cartographic Center (NCC) of Iran to measure earthquake-induced vertical displacements along the leveling line that crosses the area (Fig. 1). The level route consists of 19 stations. It runs southeast from Darzin, $\sim$30 km west of the Bam city, crosses the cities of Bam and Baravat, and continues up to about 15 km east of Baravat. The 1988 campaign was conducted

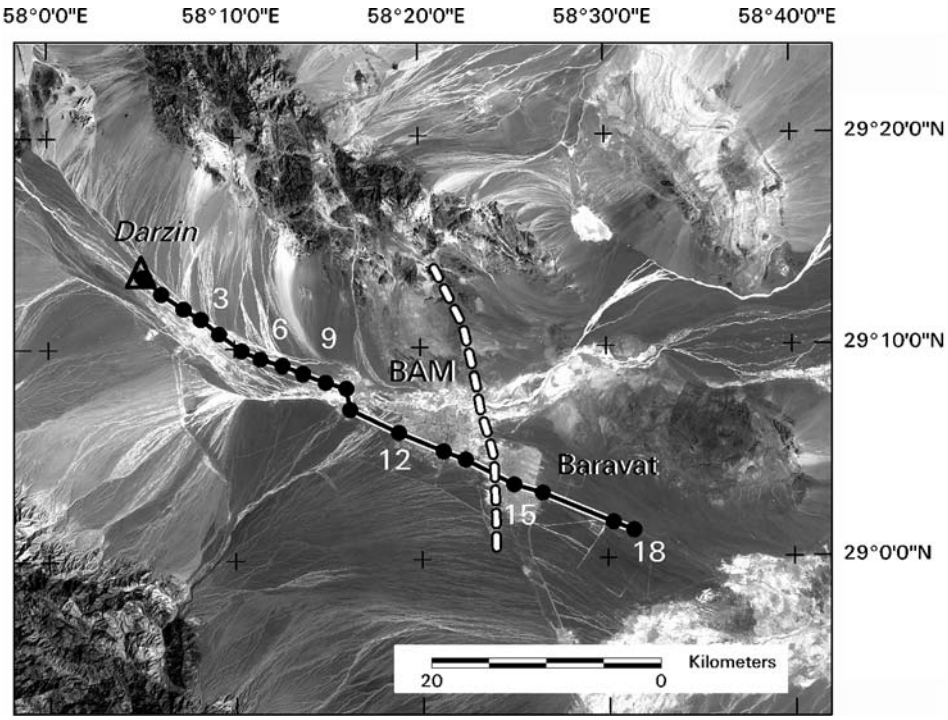

Figure 1
The leveling line (solid) as part of the Iranian first-order leveling network used in this study. Circles show the location of leveling benchmarks. The elevation changes are referenced to the westernmost station Darzin, located ~30 km from Bam. Dashed line indicates the geological Bam fault between the cities of Bam and Baravat.

using optical Wild N3 levels while in 2004 DiNi 12 digital levels were used instead. The measurement threshold throughout the two field campaigns was $3 \times S[\mathrm{km}]^{1/2}$ mm, where S is the distance in kilometers between benchmarks.

Figure 2 shows the coseismic vertical displacements with error bars of one standard deviation (Table 1). The westernmost station, Darzin, is selected as the reference point for the two campaigns. The error bars are computed based on MEMARZADEH (1998), who evaluated an average precision of $\eta = 0.7$ mm km$^{-1/2}$ for sections 1–5 km long in the Iranian first-order leveling network. Thus, the one-sigma error for detected vertical changes can be computed as:

$$\sigma_i = \pm\sqrt{2}\eta\sqrt{L_i} = \pm 0.98\sqrt{L_i}, \tag{1}$$

where L_i is the total distance along the leveling line from the reference benchmark to the ith benchmark, and σ_i is the standard deviation. As seen in Figure 2, the largest vertical uplift amounts to 12 cm at a benchmark located southwest of the Bam city (benchmark 12). The largest coseismic subsidence occurs southeast of Bam and it

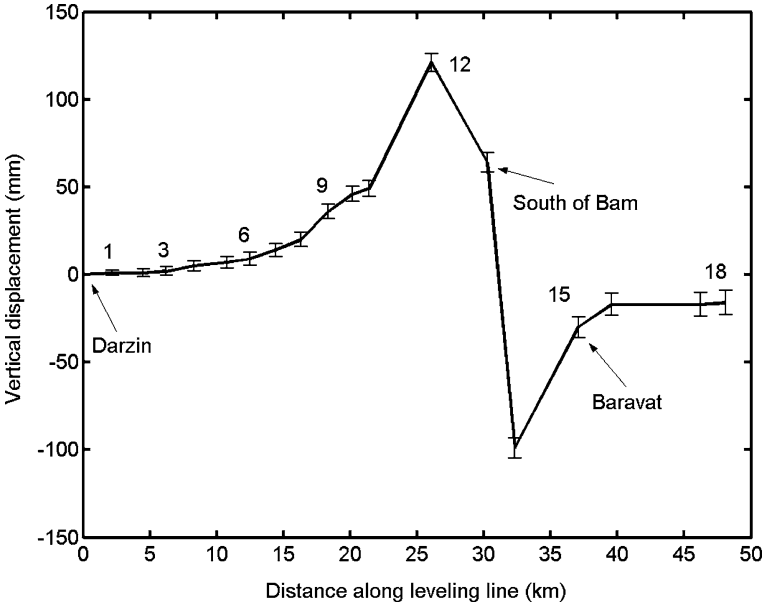

Figure 2
Coseismic elevation changes, relative to Darzin, measured after the Bam earthquake. Error bars indicate one standard deviation, $\sigma_i = \pm 0.98\sqrt{L_i}$, where L_i is the distance along the leveling line from the reference benchmark to the I-th benchmark.

reaches 10 cm (benchmark 14). South of the Bam city sustained an average uplift of about 6 cm during the event (benchmark 13). The coseismic subsidence at the village of Baravat is estimated at 3 cm. Westernmost sections located 25–30 km away from the Bam city showed no evidence of the significant amount of vertical motion between 1988 and 2004. To the east, however, approximately 1.7 cm subsidence was measured at stations 15 km away from Baravat.

The vertical displacements shown in Figure 2 include the effect of accumulated interseismic deformation between 1988 and 2004, as well as postseismic relaxation that occurred after the earthquake. The campaign-mode GPS observations do not exhibit the evidence for postseismic deformation after the event (DJAMOUR, 2003). As a result no postseismic correction is applied to measurements. For the interseismic correction, however, no reliable estimates of the long-term deformation rate are yet available for individual faults within this area. The Bam fault itself is believed to have been seismically inactive during the last two millennia (AMBRASEYS and MELVILLE, 1982). Recent GPS measurements across Iran clearly indicate that a dextral shear of 16 ± 2 mm/yr is occurring between central Iran and Afghanistan (VERNANT *et al.*, 2004). However, the precise distribution of this deformation between different tectonic structures in the region is not well constrained. Assuming that the shear

Table 1

Station coordinates and vertical coseismic displacements relative to Darzin

Station	Latitude (°)	Longitude (°)	Height (m)	Vertical displacement (m)
Darzin	29.2233	58.085	1394.995	0
1	29.21	58.1017	1367.3142	0.001
2	29.1983	58.1216	1340.205	0.001
3	29.19	58.1366	1319.569	0.002
4	29.1783	58.1533	1299.853	0.005
5	29.165	58.1733	1272.935	0.007
6	29.1583	58.19	1243.367	0.009
7	29.1533	58.21	1219.327	0.014
8	29.1467	58.2283	1201.122	0.02
9	29.14	58.2483	1181.738	0.036
10	29.135	58.2667	1161.404	0.046
11	29.1183	58.27	1153.586	0.049
12	29.1	58.3133	1114.165	0.121
13	29.085	58.3533	1075.207	0.064
14	29.0783	58.3733	1046.350	−0.099
15	29.0583	58.4166	983.381	−0.03
16	29.0517	58.4417	954.112	−0.017
17	29.0283	58.505	897.214	−0.017
18	29.0217	58.5233	882.559	−0.016

strain in this region is purely horizontal and our vertical measurements are insensitive to the regional deformation, we consider observed vertical motions in Figure 2 to be caused mainly by the $M_w = 6.5$ Bam earthquake on December 26, 2003.

2.2 INSAR Data

The synthetic aperture radar (SAR) data used in this study consists of images collected by the European Space Agency (ESA) Envisat spacecraft on 3 December 2003 and 7 January 2004 (Descending pass, Track 120, Frames: 22 and 23, orbits: 9192 and 9693) and on 16 November 2003 and 29 February 2004 (Ascending pass, Track 385, Frames: 21 and 24, orbits: 8956 and 10459). Data are processed using the public domain SAR processor DORIS developed at Delft Institute for Earth-Oriented Space Research (DEOS), Delft University of Technology (KAMPES and USAI, 1999). The software performs all the main stages of interferometric processing, from coregistration of SLC images to producing complex interferograms and coherence maps. Two-pass interferometry (MASSONNET *et al.*, 1993) is employed to isolate the deformation signal from the topographic phase contribution. We use precise DEOS satellite orbits (SCHARROO and VISSER, 1998), to model and remove the phase caused by the orbital separation of the two images and the topography. To quantify the effect of topography we use the altitude of ambiguity (h_a) defined as the amount of topography needed to produce one topographic fringe (MASSONNET and RABAUTE, 1993). For the descending pair this value is about 16 m at the image

center; therefore every 16 m of unaccounted topography would produce a 2π phase shift in the resulting interferogram. We use 3-arcsecond (90 m) resolution SRTM digital elevation model (http://seamless.usgs.gov/website/seamless/products/srtm3arc.asp) to model and remove contributions of topography to apparent range changes in the descending interferogram. The ascending pair, however, has a small orbital separation which results in the altitude of ambiguity of about 460 m at the image center. Therefore, no topographic correction is applied to this pair. The resulting interferograms are then filtered using a weighted power spectrum technique (GOLDSTEIN and WERNER, 1998) to produce the wrapped images shown in Figure 3.

Each color cycle in Figure 3a–b corresponds to approximately 2.8 cm of apparent range change between the spacecraft and the Earth's surface, that is, the component of displacement vector pointing towards the satellite. Figure 3a shows an

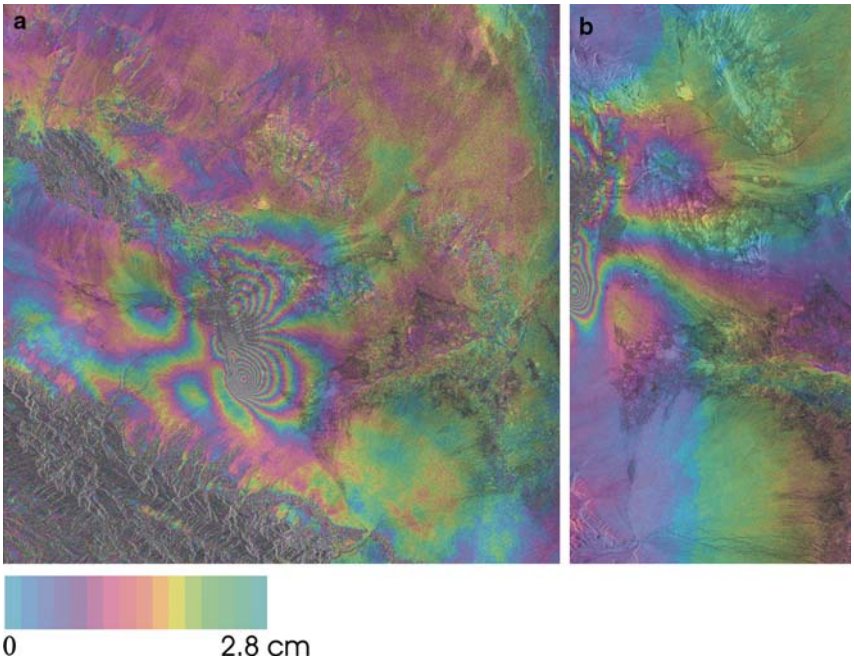

Figure 3
Coseismic displacements mapped by InSAR: (a) Descending interferogram, (b) Ascending interferogram. The asymmetric fringe pattern in the middle of the descending interferogram and the concentric fringes on the left edge of the ascending interferogram are caused by the Bam earthquake. The ascending interferogram also indicates two areas extending to 2.8 cm of range increase and range decrease SE and NE of the concentric fringes, respectively.

asymmetric fringe pattern in the middle, with about 17 cm of range increase (6 color fringes) in the northeast and 25 cm of range decrease (9 color fringes) in the southeast. Unlike the descending interferogram, however, the ascending image only captures parts of the coseismic displacement field, showing ~14 cm of range decrease on the western edge of the interferogram. It also indicates two areas of up to 2.8 cm of range increase and range decrease SE and NE of the concentric fringes, respectively.

The phase of each pixel shown above is a measure of the range change *modulo* 2π between the ground and the satellite. These observations need to be integrated to determine the total values of the phase difference at each pixel (Phase Unwrapping). We use an automated unwrapper package Snaphu (CHEN and ZEBKER, 2001) to unwrap interferograms. Because of the dry environmental condition, the coherence of the interferograms is generally high which results in reliable unwrapping. The results are then geocoded, digitized, via applying a median filter over 1 km by 1 km cells across the unwrapped interferograms, and converted from cycles into millimeters of range changes in the ground-to-satellite direction. The final data set consists of 3806 data triplets (2091 for the descending and 1715 for the ascending interferogram), containing latitude, longitude and range change in millimeters.

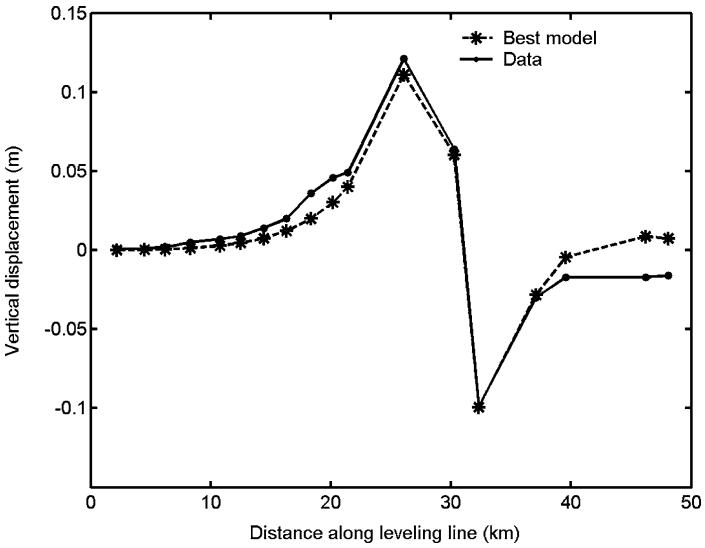

Figure 4
Modeled (dashed curve) and observed (solid curve) coseismic elevation changes as a function of distance along the leveling route.

3. Inversion for Source Parameters

3.1 Rupture Geometry

We model the observed coseismic deformation by a rectangular dislocation with uniform slip embedded in a homogeneous, isotropic, elastic half-space (OKADA, 1985). We use a constrained nonlinear optimization algorithm (BÜRGMANN *et al.*, 2002) to estimate fault parameters (fault length along strike, down-dip width, dip, depth, strike, location of the fault, and the amount of slip) that provide the best fit to the precise leveling and InSAR data. Our inversion attempts to minimize the weighted residual sum of squares $WRSS = (\mathrm{d_{obs}} - \mathrm{d_{mod}})^{\mathrm{T}} \times \Sigma^{-1} \times (\mathrm{d_{obs}} - \mathrm{d_{mod}})$, where $\mathrm{d_{obs}}$ and $\mathrm{d_{mod}}$ are the observed and modeled displacements, respectively, and Σ^{-1} is the inverse of the data covariance matrix, the so-called weight matrix. The covariance of InSAR range change measurements is not well constrained (HANSSEN, 2001; MASSONNET *et al.*, 1993), but we model the subsampled InSAR data as independent observations with 28-mm standard deviation. Vertical displacement data, however, are considered correlated with the weight matrix (ARNADOTTIR *et al.*, 1992):

$$\begin{aligned} \sum\nolimits_{i,i}^{-1} &= \frac{1}{2\sigma^2}\left[\frac{1}{L_i - L_{i-1}} + \frac{1}{L_{i+1} - L_i}\right] \\ \sum\nolimits_{i-1,i}^{-1} &= -\frac{1}{2\sigma^2}\left[\frac{1}{L_i - L_{i-1}}\right] \\ \sum\nolimits_{i,i+1}^{-1} &= -\frac{1}{2\sigma^2}\left[\frac{1}{L_{i+1} - L_i}\right] \end{aligned} \tag{2}$$

where L_i is the total distance along the leveling line from the reference benchmark to the i-th benchmark, $\Sigma_{i,j}$ is the component of the weight matrix, and σ is a constant depending on the precision of the measurement.

Initially we solved for both strike-slip and dip-slip on the fault while constraining the lower and upper bounds of the strike, dip, length and width of the fault to lie within values (−10°, 10°), (−60°, 60°), (10, 20) km, and (6, 10) km, respectively. (The positive value for the dip angle indicates dipping to the east and vice versa.) However, the dip-slip was found insignificant in the inversion and subsequently fixed to zero. We found that the best-fitting dislocation model predicts a rectangular fault 11.07 ± 0.1 by 7.9 ± 0.3 km which strikes N1.8°W ± 0.3° and dips steeply to the east (dip 88.8° ± 0.8°). The optimal fault has a centroid depth of 5.6 ± 0.03 km and slipped up to 2.5 ± 0.01 m right-lateral. The surface projection of the fault is centered at 29.043°N ± 0.03 km and 58.360°E ± 0.01 km, approximately 4 km east of the previously-mapped Bam fault. The uncertainties we report here for parameters represent approximately 95% confidence intervals computed using the classical F-test (MENKE, 1989). The estimated geodetic moment, $M_0 = \mu AS$, is 6.79×10^{18} Nm,

where A is the fault area, S is slip, and $\mu = 30$ GPa is the shear modulus. Model interferograms and leveling predictions calculated from this single-fault model resemble data well (Figs. 4 and 5a–5b). The largest residual for precise leveling data amounts to 2.5 cm on the two easternmost stations. These stations are several focal depths away from the rupture area, so their motion is probably not caused by the earthquake and we would not expect a perfect fit between the model and that part of data. For the InSAR data the residuals are largest close to the fault trace (Figs. 5c–5d). The maximum residual for both interferograms amounts to about 6 cm. Our measure of misfit which accounts for the number of model parameters P and number of data N, $\sqrt{WRSS/(N-P)}$, is 0.7, indicating that adequate fitting of the model to

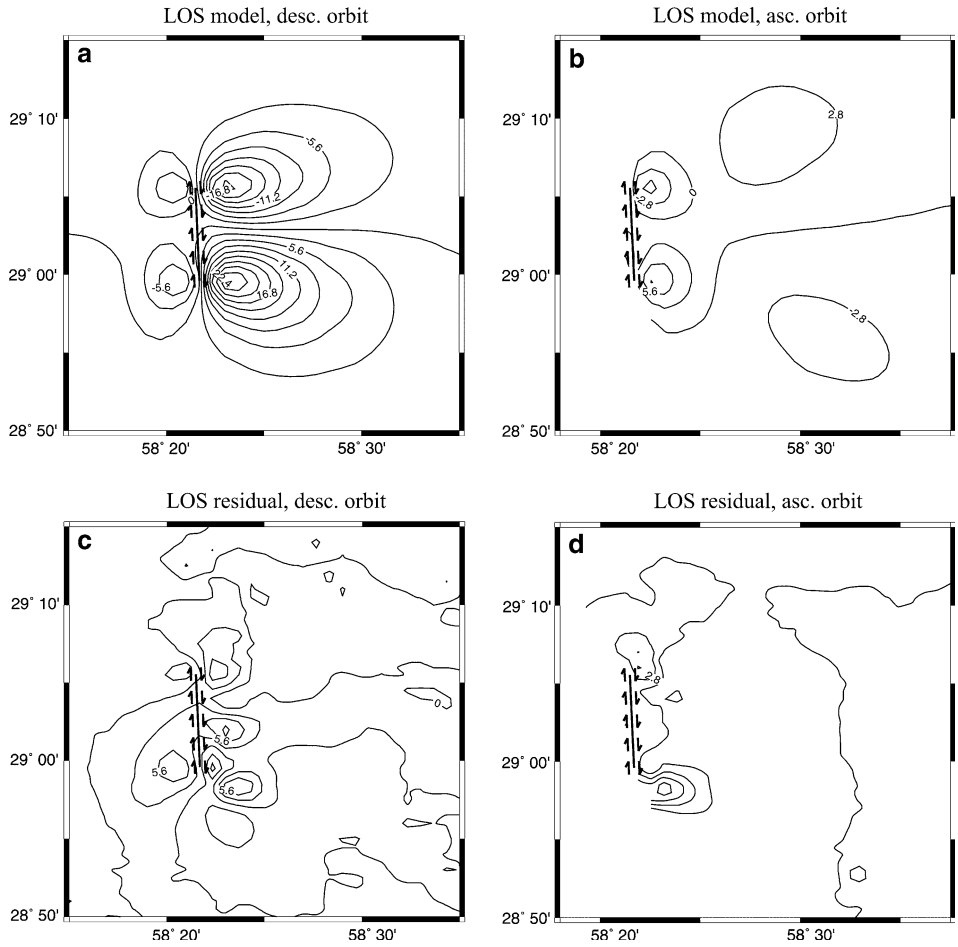

Figure 5
(a,b) Best-fitting InSAR models. (c,d) Residuals obtained by subtracting the model predictions from the data. Contours indicate line-of-sight displacements at 2.8 cm intervals. Black solid line is the fault trace used in modeling. Solid arrows show the shear dislocation for the right-lateral strike-slip fault.

the data has been achieved (MENKE, 1989; AYHAN *et al.*, 2001; PEDERSEN *et al.*, 2003).

3.2 Slip Distribution

To investigate the possibility of resolving more detailed information on the coseismic rupture plane, we enlarge the best-fitting single-fault model determined above at the down-dip and lateral edges and parameterize it by a two-dimensional grid of rectangular elements. Because of limited resolving power of surface deformation data in identifying fine-scale slip features on deep patches (BOS and SPAKMAN, 2003; DU *et al.*, 1992), we increase the cell size with depth, starting with approximately 500 m by 500 m cells for the uppermost patches. The patch size increases to 1, 2 and 4 km for deeper subfaults. Using a fixed geometry, surface deformation data d can be expressed as a linear function of slip distribution s on the fault:

$$d = Gs + \varepsilon, \tag{3}$$

where G consists of the synthetic Green's functions (surface displacements calculated for 1 m of slip on each fault patch using OKADA (1985) formulation) and ε is the measurement error. We use a standard linear least-squares inversion to solve the above equation and seek an estimate of the slip s that minimizes the function

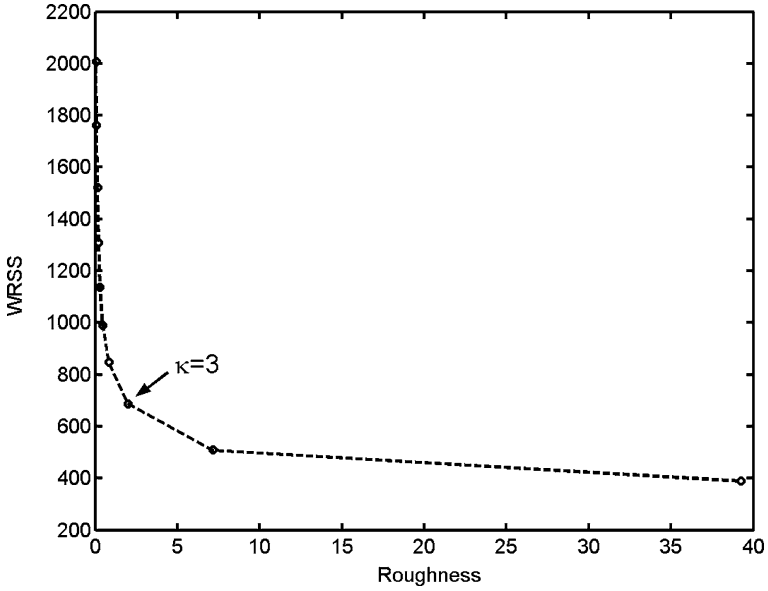

Figure 6
Plot of WRSS versus the roughness of the estimated slip for a range of smoothing factors. $\kappa = 3$ was selected as the penalty factor for the slip inversion.

$$\phi = \left\| \Sigma^{-1/2}(G\vec{s} - \vec{d}) \right\| + \kappa^2 \left\| \nabla^2 \vec{s} \right\| \quad \text{Subject to } s_i \geq 0, \tag{4}$$

where the first term is the weighted residual sum of squares (WRSS) and the second term is a measure of roughness of solution defined as finite difference approximation of the Laplacian of slip (HARRIS and SEGALL, 1987). The penalty factor κ is introduced in the inversion to control the smoothing constraint. The slip is confined to be positive, so that only solutions with right-lateral strike-slip are allowed.

To determine the penalty factor κ, we follow the lead of previous studies (BÜRGMANN *et al.*, 2002; ARNADOTTIR and SEGALL, 1994) and plot a trade-off curve to find out the relative weight between the fit to the data and the model complexity. Figure 6 shows WRSS as a function of model roughness $\left\| \nabla^2 \vec{s} \right\|$. Based on the trade-off curve we select κ equal to 3, beyond which we do not observe a substantially better fit to data at the expense of increasing the model roughness. Figure 7 shows the strike-slip model for the Bam earthquake which we derive from the inversion of InSAR and leveling data. The slip pattern is relatively homogeneous with coseismic slip reaching a maximum around the fault center. The slip and depth of faulting taper to the north, where the rupture approaches the city of Bam. The highest coseismic

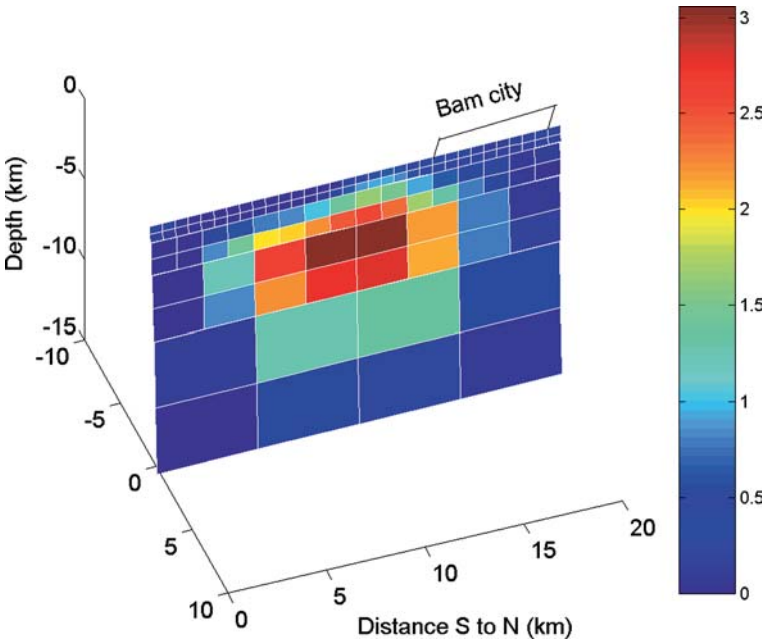

Figure 7
Slip distribution model on the coseismic fault plane from the joint inversion of InSAR and leveling data. The uppermost cell size of the grid is 0.5 by 0.5 km. The cell size increases to 1, 2 and 4 km for deeper subfaults. The parallelogram specifies the approximate location of the Bam city. The highest coseismic slip reaches 3 m at a depth of about 3 to 5 km.

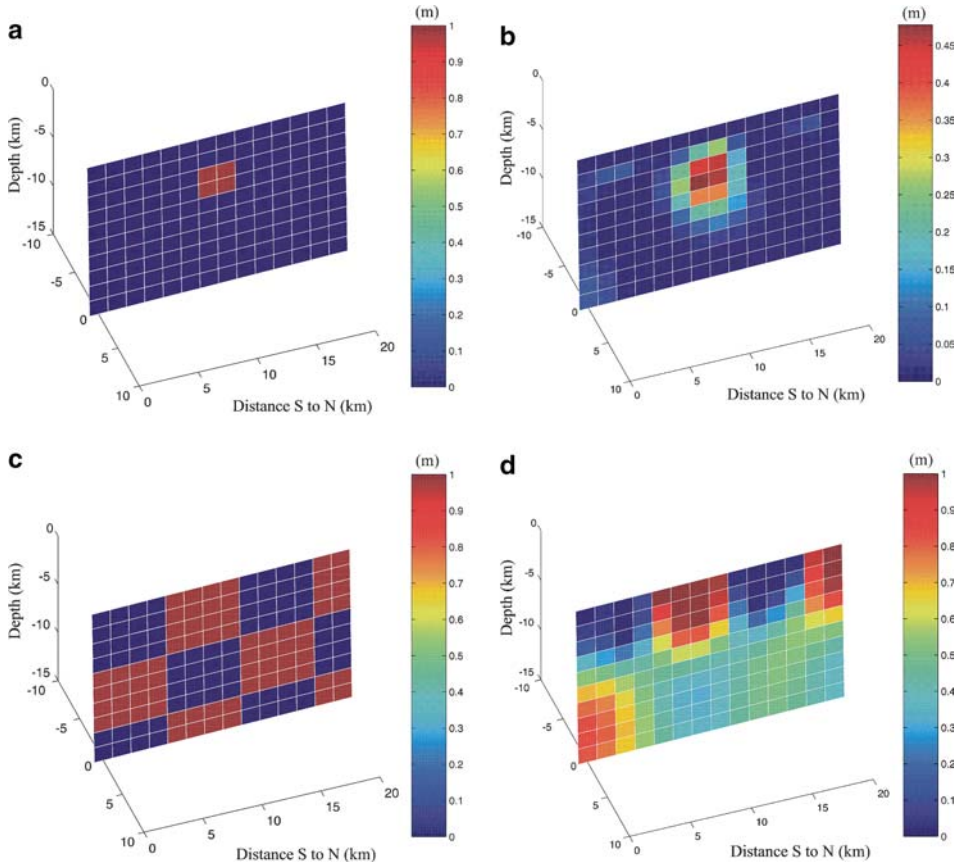

Figure 8
The resolution analysis for the distributed slip model; patches are 1.5 km by 1.5 km: (a,b) A spike test model, (c,d) a checkerboard test model.

slip occurs at a depth of about 3 to 5 km and it reaches up to 3 m. The slip model predicts very little to no dextral offset for the uppermost patches, consistent with scant surface ruptures observed in the field (TALEBIAN, 2004). There is no significant coseismic slip on the section of the fault below a depth of 9 km. Our slip distribution model, however, provides only a slightly better fit to the data than the uniform slip model (results not shown here), suggesting that the Bam event might indeed be a rather simple rupture.

3.3 Model Resolution

Any estimation of the slip distribution based on surface deformation data suffers from providing reliable fine-scale slip values for deep patches on the fault. To address this issue and assess the ability of our inversion in recovering the correct slip model,

we perform a resolution analysis by generating some synthetic surface displacement data for the two known slip models shown in Figures 8a and 8c; the so-called spike and checkerboard model, respectively. We add independent noise to the synthetic data from both models and invert them using the same method described above to retrieve the fault slip. The recovered solutions for the spike and checkerboard model are shown in Figures 8b and 8d, respectively. Figure 8b illustrates how our inversion might smear information about one patch into some of adjacent patches, resulting in a model with the maximum slip amplitude of about 50% of the correct slip amplitude. Figure 8d recovers some essential features of the true slip model, particularly for shallow patches, but is not able to provide sufficient information on the spatial wavelength of the slip distribution at depth greater than 6 km. The lack of sufficient resolving power becomes more severe at larger depths, prohibiting us from retrieving reliable information about the details of the deep fault slip from surface deformation data.

3.4 Crustal Layering

Inversions of geodetic data for fault slip frequently rely on elastic half-space models. These models, however, do not allow us to consider the effect of rigidity layering on slip models. Here, we also tested the inversion in a more realistic Earth model by incorporating a depth-dependent rigidity structure proposed by ZOHOORIAN *et al.* (1984) for the Bam area (Table 2). We used EDGRN code (WANG *et al.*, 2003) to compute the synthesized Green's functions for the layered Earth model and followed the same strategy as in Section 3.2 to find slip values most consistent with geodetic data. The slip pattern resulted from the layered half-space Earth model showed very little discrepancy with that derived from the elastic half-space model. Rigidity stratification increased the amount of maximum coseismic slip inferred at depth by about 4%. This value can be neglected, taking into account the low resolution of our inversion scheme on deep patches. This confirms that the slip model we obtained in this study is not drastically distorted by artifacts of Earth structure (SAVAGE, 1987; SIMONS *et al.*, 2002).

Table 2

Horizontal layer structure based on ZOHOORIAN et al. (1984)

Layer	Vp (km/s)	Vs (km/s)	ρ (10^3 kg/m^3)	D (km)
1	5.00	2.89	2.6	0–6
2	5.50	3.18	2.6	6–16
3	6.50	3.75	2.6	16–41
4	8.00	4.62	2.6	41–∞

4. Discussion and Conclusions

Geodetic data rule out that the Bam earthquake occurred on the previously-mapped Bam fault, as suggested by HESSAMI *et al.* (2004), FU *et al.* (2004) and ZARE and HAMZEHLOO (2004). The coseismic surface displacements calculated from the combination of precise leveling and radar interferometric observations can be best explained by a near-vertical strike-slip fault rupturing an area of about 11 by 8 km south of the city of Bam. The dislocation strikes N2°W and has an average right-lateral strike-slip component of 2.5 m. Using a reference shear modulus (30 GPa), we find geodetic moment 6.79×10^{18} Nm, similar to seismic estimates of 6.6×10^{18} Nm (fast moment tensor solution; USGS (2003)), and 6.8×10^{18} Nm (teleseismic inversion; YAGI (2003)). Our slip distribution model suggests that the largest amount of coseismic slip occurs at a depth of about 3 to 5 km, where it reaches up to 3 m. The slip magnitude and depth of faulting decrease towards the north, where the fault approaches the city. This model, however, is not consistent with the teleseismic inversions of YAGI (2003), who identified three asperities corresponding to the Bam event with maximum dislocation of 1.2 m at a depth of about 10 km.

TALEBIAN *et al.* (2004) used InSAR data in descending orbit to estimate source parameters of the Bam earthquake. TALEBIAN *et al.* (2004) concluded that a combination of two events, a major strike-slip fault (strike 357°, dip 88°, rake −166°) followed by a pure thrust fault (strike 180°, dip 30°, rake 90°), is necessary to fit InSAR observations. The main strike-slip dislocation in TALEBIAN *et al.* (2004) is located approximately 5 km west of the previously-mapped Bam fault, while the surface projection of the secondary dislocation lies at a distance of about 10 km east of the main rupture. WANG *et al.* (2004) used descending and ascending interferograms and constructed a source model based on three rectangular faults, rupturing a total length of about 24 km from south to north crossing the Bam city. WANG *et al.* (2004) concluded that more than 80 percent of seismic moment was released from a new dislocation located 4–5 km west of the Bam fault dipping 80°E. WANG *et al.* (2004) found no evidence for secondary thrust dislocation as proposed by TALEBIAN *et al.* (2004).

The size and the strike of the southern segment in WANG *et al.* (2004) as well as the first mechanism considered by TALEBIAN *et al.* (2004) for the main rupture agree well with our estimates. However, the joint inversion of precise leveling and InSAR data favors a fault that dips at a steeper angle than that proposed by WANG *et al.* (2004). Figure 9 shows the prediction of WANG *et al.* (2004) for the leveling data. This model leaves large residuals at benchmarks around the city of Bam (benchmarks 12–14). In contrast, our model predictions resemble vertical data well (see Fig. 4). We note that part of the discrepancy between the model we estimate and that predicted by WANG *et al.* (2004) could be due to the different methodology we used to find the source parameters. Noticeably, WANG *et al.* (2004) used the trial-and-error method which is less effective than our nonlinear inversion algorithm in searching for a

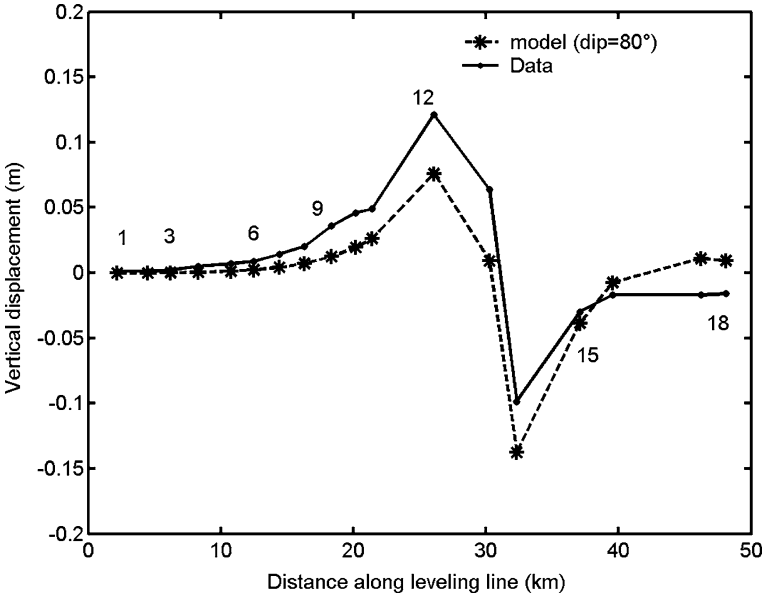

Figure 9
Prediction of leveling data based on WANG *et al.* (2004). This model leaves large residuals at benchmarks around the city of Bam (benchmarks 12–14).

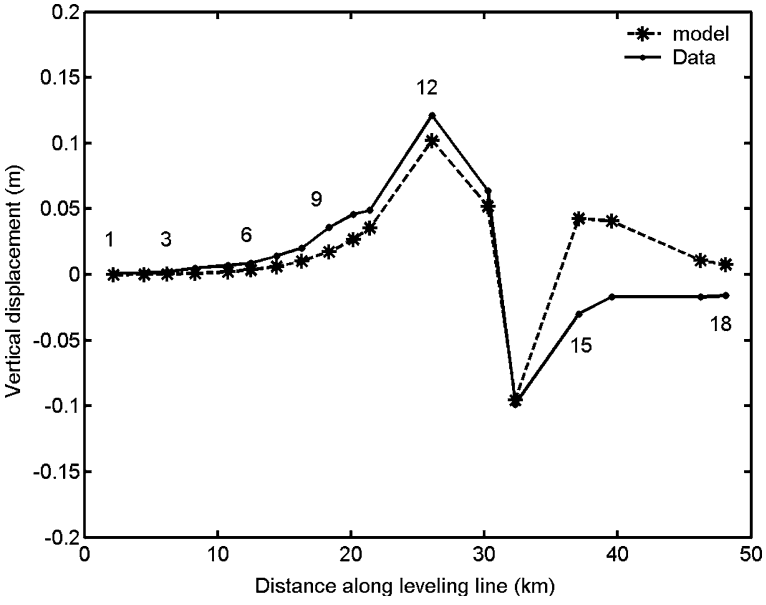

Figure 10
Prediction of leveling data when a secondary shallow dislocation is introduced beneath the previously-mapped Bam fault. This model leaves large residuals at benchmarks on the east side of the main rupture (benchmarks 15–16).

solution. Furthermore, inclusion of precise leveling data enabled us to decrease the number of possible candidates in the solution space, leading to a more reliable estimate of source parameters.

Unlike TALEBIAN *et al.* (2004) our analysis does not verify the existence of a secondary shallow dislocation beneath the previously-mapped Bam fault. Introduction of such a dislocation does not provide a good fit to vertical displacements (see Fig. 10), particularly at benchmarks on the east side of the main rupture (benchmarks 15–16). This indicates that the Bam event did not cause any secondary shallow slip on the geological Bam fault.

Acknowledgements

We are grateful to many individuals at the National Cartographic Centre of Iran who contributed to the acquisition of the leveling data. We acknowledge the cooperation of the European Space Agency for providing Envisat ASAR data. Many thanks go to Roland Bürgmann for generously providing us with scripts used in dislocation modeling. We would like to thank Tim Wright and an anonymous referee for their reviews and insightful comments. Figure 5 was produced by the public-domain software GMT (WESSEL and SMITH, 1991).

REFERENCES

AMBRASEYS, N.N. and MELVILLE, C.P., *A History of Persian Earthquakes*, (Cambridge University Press, London, 1982).

ARNADOTTIR, T., SEGALL, P., and MATHEWS, M. (1992), *Resolving the discrepancy between geodetic and seismic fault models for the 1989 Loma Prieta, California, earthquake*, Bull. Seismol. Soc. Am. *82*, 2248–2255.

ARNADOTTIR, T. and SEGALL, P. (1994), The *1989 Loma Prieta earthquake imaged from the inversion of geodetic data*, J. Geophys. Res. *99*, 21,835–21,855.

AYHAN, M.E., BÜRGMANN, R., MCCLUSKY, S., LENK, O., AKTUG, B., HERECE, E., and REILINGER, R.E. (2001), *Kinematics of the M_w 7.2, 12 November 1999, Düzce, Turkey earthquake*, Geophys. Res. Lett. *28*, 367–370.

BERBERIAN, M., JACKSON, J.A., FIELDING, E., PARSONS, B.E., PRIESTLEY, K., QORASHI, M., TALEBIAN, M., WALKER, R., WRIGHT, T.J., and BAKER, C. (2001), *The 1998 March 14 Fandoqa earthquake (M_w 6.6) in Kerman province, southeast Iran: Re-rupture of the 1981 Sirch earthquake fault, triggering of slip on adjacent thrusts and the active tectonics of the Gowk fault zone*, Geophys. J. Int. *146*, 371–398.

BOS, A.G. and SPAKMAN, W. (2003), The resolving power of coseismic surface displacement data for fault slip distribution at depth, Geophys. Res. Lett. *30*, doi:10.1029/2003GL017946.

BÜRGMANN, R., AYHAN, M.E., FIELDING, E.J., WRIGHT, T.J., MCCLUSKY, S., AKTUG, B., DEMIR, C., LENK, O., and TÜRKEZER, A. (2002), *Deformation during the 12 November 1999 Düzce, Turkey, Earthquake from GPS and InSAR Data*, Bull. Seismol. Soc. Am. *92*,161–171.

CHEN, C.W. and ZEBKER, H.A. (2001), *Two-dimensional phase unwrapping with use of statistical models for cost functions in nonlinear optimization*, J. Optical Soc. Am. (Optics, Image Science and Vision) *18*, 338–351.

DJAMOUR, Y. (2003), Personal communication.

Du, Y., AYDIN, A., and SEGALL, P. (1992), *Comparison of various inversion techniques as applied to the determination of a geophysical deformation model for the 1983 Borah Peak earthquake*, Bull. Seismol. Soc. Am. *82*, 1840–1866.

GABRIEL, A.K., GOLDSTEIN, R.M., and ZEBKER, H.A. (1989), *Mapping small elevation changes over large areas: Differential radar interferometry*, J. Geophys. Res. *94*, 9183–9191.

GOLDSTEIN, R.M. and WERNER, C.L. (1998), *Radar interferogram filtering for geophysical Application,* Geophys. Res. Lett. *25*, 4035–4038.

HANSSEN, R., *Radar Interferometry: Data interpretation and Error Analysis* (Kluwer Academic Publishers, Netherlands, 2001).

HARRIS, R.A. and SEGALL, P. (1987), *Detection of a locked zone at depth on the Parkfield, California, segment of the San Andreas fault*, J. Geophys. Res. *92*, 7945–7962.

HESSAMI, K., TABASSI, H., ABBASSI, M.R., AZUMA, T., OKUMURA, K., ECHIGO, T., and KONDO, H. (2004), *Surface expression of the Bam fault zone in southeastern Iran: Causative fault of the 26 December 2003 Bam earthquake*, J. Seismol. Earthq. Engin. Special Issue on Bam Earthquake, 5–14.

KAMPES, B. and USAI, S. (1999), ''Doris: The Delft Object-oriented Radar Interferometric software.'' In Proceedings ITC 2nd ORS Symposium.

MASSONNET, D. and RABAUTE, J. (1993), *Radar interferometry: limits and potential*. IEEE Transact. Geosci. Remote Sensing *31*, 455–464.

MASSONNET, D., ROSSI, M., CARMONA, C., ADRAGNA, F., PELTZER, G., FEIGL, K., and RABAUTE, T. (1993), *The displacement field of the Landers earthquake mapped by radar interferometry*, Nature *364*, 138–142.

MEMARZADEH, Y. (1998), *Refraction Effect and Statistical Analysis of the Iran First Order precise Leveling Data*, Master Thesis, K.N.Toosi University of Technology.

MENKE, W., *Geophysical Data Analysis: Discrete Inverse Theory, Revised Edition* (Academic Press, Inc., New York, 1989).

MOSTAFAZADEH, M., FARAHBOD, M., MOKHTARI, M., and ALLAMEHZADEH, M. (2004), *Seismological Aspect of 26 December 2003 Bam Earthquake*, J. Seismol. Earthq./ Engin. Special Issue on Bam earthquake, 15–21.

OKADA, Y. (1985), *Surface deformation due to shear and tensile faults in a half-space*, Bull. Seismol. Soc. Am. *75*, 1135–1154.

PEDERSEN, P., JÓNSSON, S., ÁRNADÓTTIR, T., SIGMUNDSSON, F., and FEIGL, K. (2003), *Fault slip distribution of two June 2000 M_w 6.5 earthquakes in South Iceland from joint inversion of InSAR and GPS*, Earth Plan Sci. Lett. *213*, 487–502.

SAVAGE, J. C. (1987), *Effect of crustal layering upon dislocation modeling,* J. Geophys. Res. *92*, 10595–10600.

SCHARROO, R. and VISSER, P.N.A.M. (1998), *Precise orbit determination and gravity field improvement for the ERS satellites*, J. Geophys. Res. *103*, 8113–8127.

SIMONS, M., FIALKO, Y., and RIVERA, L. (2002), *Coseismic deformation from the 1999 M_w 7.1 Hector Mine, California, Earthquake as inferred from InSAR and GPS observations*, Bull. Seismol. Soc. Am. *92*, 1390–1402.

TALEBIAN, M., FIELDING, E.J., FUNNING, G.J., GHORASHI, M., JACKSON, J.A., NAZARI, H., PARSONS, B., PRIESTLEY, K., ROSEN, P.A., WALKER, R., and WRIGHT, T.J. (2004), *The 2003 Bam (Iran) earthquake: Rupture of a blind strike-slip fault*, Geophys. Res. Lett. *31*(11), L11611, doi:10.1029/2004GL020058.

TATAR, M., HATZFELD, D., MORADI, A.S., PAUL, A., FARAHBOD, A.M., and MOKHTARI, M. (2004), *Aftershock study of the 26 December 2003 Bam earthquake*, J. Seismol. Earthq. Engin., Special Issue on Bam Earthquake, 23–31.

USGS (2003), *http://neic.usgs.gov/neis/eq_depot/2003/eq_031226/neic_cvad_q.html*

VERNANT, P., NILFOROUSHAN, F., HATZFELD, D., ABBASI, M.R., VIGNY, C., MASSON, F., NANKALI, H., MARTINOD, J., ASHTIANI, A., BAYER, R., TAVAKOLI, F., and CHÉRY, J. (2004), *Contemporary crustal deformation and plate kinematics in Middle East constrained by GPS measurements in Iran and northern Oman*, Geophys. J. Int. *157*, 381–398.

WANG, R., LORENZO MARTÍN, F., and ROTH, F. (2003), *Computation of deformation induced by earthquakes in a multi-layered elastic crust - FORTRAN programs EDGRN/EDCMP*, Computers and Geosciences *29*, 195–207.

WANG, R., XIA, Y., GROSSER, H., WETZEL, H.-U., ZSCHAU, J., and KAUFMANN, H. (2004), *The 2003 Bam (SE Iran) earthquake: Precise source parameters from satellite radar Interferometry*, Geophys. J. Int. *159*, 917–922.

WESSEL, P. and SMITH, W.H F. (1991), *Free Software Helps Map and Display Data,* EOS Trans., AGU, *72*, 441.

YAGI, Y. (2003), *http://iisee.kenken.go.jp/staff/Yagi/eq/Iran20031226/IRAN20031226.htm*

ZARÉ, M. and HAMZEHLOO, H. (2004), *A Study of the strong ground motions of 26 December, 2003 Bam Earthquake: M_w 6.5*, J. Seismol. Earthq. Engin., Special Issue on Bam Earthquake, 33–56.

ZEBKER, H.A., ROSEN, P.A., GOLDSTEIN, R.M., GABRIEL, A., and WERNER, C.L. (1994), *On the derivation of coseismic displacement fields using differential radar interferometry: The Landers earthquake,* J. Geophys. Res. *99*, 19617–19634.

ZOHOORIAN, A., MOHAJER-ASHJAI, A., KABIRI, A., and HOSSEINIAN-GHAMSARI, M. (1984), *Damage distribution and aftershock sequence of two destructive earthquakes in 1981 in eastern Kerman,* J. Earth Space Phys. *10* (1, 2).